Impact of periodic vaccination in SEIRS seasonal model FREE

Enrique C. Gabrick ✉ 🆔 ; Eduardo L. Brugnago 🆔 ; Silvio L. T. de Souza 🆔 ; Kelly C. Iarosz 🆔 ;
José D. Szezech, Jr. 🆔 ; Ricardo L. Viana 🆔 ; Iberê L. Caldas 🆔 ; Antonio M. Batista 🆔 ; Jürgen Kurths 🆔

Check for updates

CrossMark

View Online

Export Citation

Chaos

Special Topic:
Nonautonomous Dynamical Systems:
Theory, Methods, and Applications

Submit Today

AIP Publishing

Impact of periodic vaccination in SEIRS seasonal model

Enrique C. Gabrick,[1,2,3,a)]   Eduardo L. Brugnago,[4]   Silvio L. T. de Souza,[5]   Kelly C. Iarosz,[3,6]   José D. Szezech, Jr.,[3,7]   Ricardo L. Viana,[4,8]   Iberê L. Caldas,[4]   Antonio M. Batista,[3,4,7]   and Jürgen Kurths[1,2]
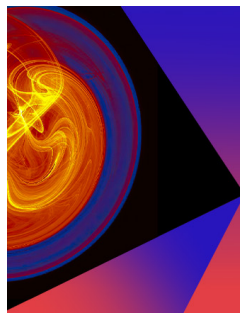
AFFILIATIONS

[1] Potsdam Institute for Climate Impact Research, Telegrafenberg A31, 14473 Potsdam, Germany
[2] Department of Physics, Humboldt University Berlin, Newtonstraße 15, 12489 Berlin, Germany
[3] Graduate Program in Science, State University of Ponta Grossa, 84030-900 Ponta Grossa, PR, Brazil
[4] Institute of Physics, University of São Paulo, 05508-090 São Paulo, SP, Brazil
[5] Federal University of São João del-Rei, Campus Centro-Oeste, 35501-296 Divinópolis, MG, Brazil
[6] University Center UNIFATEB, 84266-010 Telêmaco Borba, PR, Brazil
[7] Department of Mathematics and Statistics, State University of Ponta Grossa, 84030-900 Ponta Grossa, PR, Brazil
[8] Department of Physics, Federal University of Paraná, 81531-980 Curitiba, PR, Brazil

[a)] **Author to whom correspondence should be addressed:** enriquec@pik-potsdam.de; ecgabrick@gmail.com

ABSTRACT

We study three different strategies of vaccination in an SEIRS (Susceptible–Exposed–Infected–Recovered–Susceptible) seasonal forced model, which are (*i*) continuous vaccination; (*ii*) periodic short-time localized vaccination, and (*iii*) periodic pulsed width campaign. Considering the first strategy, we obtain an expression for the basic reproduction number and infer a minimum vaccination rate necessary to ensure the stability of the disease-free equilibrium (DFE) solution. In the second strategy, short duration pulses are added to a constant baseline vaccination rate. The pulse is applied according to the seasonal forcing phases. The best outcome is obtained by locating intensive immunization at inflection of the transmissivity curve. Therefore, a vaccination rate of 44.4% of susceptible individuals is enough to ensure DFE. For the third vaccination proposal, additionally to the amplitude, the pulses have a prolonged time width. We obtain a non-linear relationship between vaccination rates and the duration of the campaign. Our simulations show that the baseline rates, as well as the pulse duration, can substantially improve the vaccination campaign effectiveness. These findings are in agreement with our analytical expression. We show a relationship between the vaccination parameters and the accumulated number of infected individuals, over the years, and show the relevance of the immunization campaign annual reaching for controlling the infection spreading. Regarding the dynamical behavior of the model, our simulations show that chaotic and periodic solutions as well as bi-stable regions depend on the vaccination parameters range.

Published under an exclusive license by AIP Publishing. https://doi.org/10.1063/5.0169834

The spread of infectious diseases is a challenge to world public health. Many efforts are dedicated to mitigating the impacts of the spreading of diseases. In this context, a mathematical model is a powerful tool to simulate, forecast, and study efficient control measures for human and wildlife diseases. Although there are many types of diseases, some of them have common characteristics, for instance, to repeat the peak of infectious in certain times. These diseases are called seasonal, e.g., measles, mumps, and smallpox. The reasons for the seasonality can be varied, such as climate and social behaviors. Due to the seasonal characteristics of these diseases, they recur in the populations, and control measures are needed to be implemented in order to eradicate them. One of the most successful control measure is a vaccination campaign, which can be continuous or periodic. Continuous vaccination is a campaign in which a constant quantity of vaccines is daily available to the population throughout the year, while the periodic strategy considers an intense immunization campaign, during a fraction of the year. In this work, we study the impacts of vaccination in an SEIRS model with seasonal forcing. We consider newborns vaccine and susceptible vaccination, administrated in three different ways: (i) continuous vaccination; (ii) periodic short-time localized vaccination, and (iii) periodic pulsed width campaign. For the periodic strategies, we consider a baseline rate. In the constant vaccine context, we obtain an

analytical expression for the vaccination rate in which the DFE is guaranteed. For the parameters considered, the annually vaccinated value is in agreement with numerical simulations for all the vaccine strategies. Furthermore, considering parameters for which bi-stability exist in the case without vaccine, our results show that it persists depending on the vaccination rate.

I. INTRODUCTION

Infectious diseases spreading is a highly important problem in public health.[1] The spread of infectious diseases affects the humanity throughout whole history,[2] e.g., Black Death during the fourteenth century,[2] Spanish flu in 1918,[3] COVID-19,[4] Dengue fever,[5] HIV,[6] etc.[7–9] Some of these illnesses present seasonal patterns of incidence,[10] namely, seasonal infectious diseases.[11] The mechanisms of seasonality are varied, such as weather,[12] school holidays,[13] and others.[14] Examples of seasonal infectious diseases are mumps,[15] measles,[1] and dengue fever.[16] An introduction to corresponding models is found in Refs. 10 and 11.

Mathematical models are a powerful tool for studying the spread of diseases, through predictions of new outbreaks and simulation of control measures.[17] In epidemiology, the standard models are compartmental,[18] where the host population is compartmentalized according to the stages of the infection evolution and the possible states considered. The individuals in the host population are taken from susceptible to possible intermediate stages, as infectious and recovered. Depending on the disease to be modelled, when an infection cycle is completed, the individuals can acquire permanent immunity[19] or become susceptible again. These models are easily adapted to study different diseases, as seasonal infectious ones,[20] which can be modelled by the inclusion of a nonlinear time-dependent term in the transmissivity, e.g., a sinusoidal forcing[21] or a square wave function.[22] Due to this non-linearity, the resulting dynamics can become very intricate, even exhibiting chaos[23] or bi-stability.[24]

From a modeling perspective, seasonal models have been used since 1928.[11] These models reproduce the dynamics observed in diseases, such as measles,[23] chickenpox, mumps,[25] and others,[10] with great accuracy. In a formulation of the SIRS (Susceptible–Infected–Recovered–Susceptible) model with seasonal contact rate, Greenhalgh and Moneim[26] showed the existence of a unique DFE solution, which is globally asymptotically stable when the basic reproduction number is less than one ($\mathcal{R}_0 < 1$), where $\mathcal{R}_0$ is a measure of the reproductive potential for a given disease. In a population, where everyone is initially susceptible, the infection can remain only if $\mathcal{R}_0 > 1$.[20] Furthermore, Greenhalgh and Moneim considered four childhood infectious diseases (measles, chickenpox, mumps, and rubella) and showed non-trivial solutions (chaotic dynamics). These results are found by analyzing the bifurcation diagram, where some ranges exhibit chaotic attractors. Also in an SIR (Susceptible–Infected–Recovered) framework, de Carvalho and Rodrigues[27] implemented a multi-parameter periodically forced term leading to strange attractor solutions. In their formulation, the DFE is not preserved when $\mathcal{R}_0 < 1$. Metcalf et al.[28] studied the seasonal variation of six childhood infections (measles, pertussis, mumps, diphtheria,

varicella, and scarlet fever) from the data of Copenhagen in the pre-vaccination era. Their results showed that the transmission disease decreases for some infections at school holidays.

Previous works reported the capacity of compartmental models to reproduce chaotic dynamics[29] and the accuracy in simulating real data.[4,30] However, one of the most important advantages in using compartmental models is the facility to implement important characteristics to simulate control measures, such as social distancing,[31,32] restrictive measures,[17,33] quarantine,[35,36] vaccination,[37,38] etc. Despite there are some forms of control, one of the most effective is vaccination.[36,39,40]

Vaccination campaign in infectious seasonal diseases shows a significant infected number decrease.[14,41,42] Gao et al.[43] studied the vaccination of newborns combined with pulsed vaccine in an SIRS seasonal forced model in a modeling approach. One of the results obtained in this research is the DFE when $\mathcal{R}_0 < 1$. The rotavirus vaccination was studied by Atchison et al.[44] using a modified SIR model to fit the data from England and Wales. From these simulations, they reported that vaccination reduces rotavirus diseases transmission by 61%. Considering a pulsed vaccination strategy in an SIR model, Shulgin et al.[45] showed the possibility of disease eradication with relatively low vaccination rates. To get disease eradication, they explored some conditions, as vaccine proportion and periodicity. The effects of two vaccination doses in an SEIR (Susceptible–Exposed–Infected–Recovered) epidemic model was studied by Gabrick et al.[46] In this work, they considered three vaccination strategies: unlimited doses applied continuously in the susceptible population, limited doses supply applied periodically in the susceptible population, and limited doses applied in a periodic strategy in all host population. Their results showed that the vaccine campaign is more efficient when applied only in susceptible individuals, i.e., the population is previously tested. Considering a Kot-type function as seasonality, Duarte[47] analyzed the control of infectious disease with vaccination strategies including a perturbation term. Seasonal contact and optimal vaccination strategy were studied by Wang[48] in an SEIR model. The persistence or extinction of a seasonal disease with reinfection possibility was discussed by Bai and Zhou.[49] They explored the conditions for the extinction of the diseases in the situations where $\mathcal{R}_0 < 1$ and also $\mathcal{R}_0 > 1$. Their results showed that $\mathcal{R}_0 = 1$ is the threshold for disease extinction. However, from simulations, a policy only based on $\mathcal{R}_0$ can overestimate the infections' risks and the infected number due the presence of seasonality. Periodic strategy vaccination in an SEIRS model was discussed by Moneim and Greenhalgh.[50] The vaccine periodicity was described as integer multiples of the contact rate period. They reported that a key parameter to understand the vaccine influence is the $\mathcal{R}_0$. Also, they proved that $\mathcal{R}_0 < 1$ is associated with the DFE and is globally asymptotically stable. Other works that address the vaccination of seasonal diseases can be found in Refs. 51–54 and in the references therein.

In this work, we study the effects of vaccination in an SEIRS seasonal forced model.[24,49] We substantially extended the works of Moneim and Greenhalgh[50] and Gabrick et al.[24] The first one explored the effects of periodic vaccination and conjectured one $\mathcal{R}_0$ as a function of vaccine parameters. However, the authors did not explore the effects of constant vaccine and periodic pulses with different widths. In the second one, the authors obtained a parameter

26 January 2024 00:00:50

range in which the numerical solutions exhibit bi-stability and tipping point phenomena can be explored. However, they did not taken into account the vaccine influences in the dynamical behavior. In this way, our work extend the Ref. 50 by implementing three different strategies of vaccination in susceptible and newborn individuals, namely, (i) constant, (ii) pulsed, and (iii) pulsed width vaccination strategies. We choose these three strategies because (i) it can be used to model mass vaccination programs;[55] (ii) it can be considered to model a scenario in which a certain amount of vaccination (baseline) is available during all the time, but periodically an intense campaign is employed;[56] and strategy (iii) modified (ii) by extending the duration of the intensive immunization campaign to days, weeks or months, i.e., it saves vaccination efforts. Then, considering the parameters found in Ref. 24 for bi-stability, we explore, as novelty, the dynamical aspects of the SEIRS seasonal in the presence of vaccine, according to the three strategies mentioned. Our simulations show that for the (i) case, the vaccine in susceptible is more significant and rates $\geq 44\%$ are able to extinct the infection in the host population. In the (ii) scenario, we found a linear relationship between the baseline and pulsed immunization rate to result in infection eradication. Also, acting the pulses at the inflection point of the seasonality function, the campaign is slightly more effective. To the strategy (*iii*), we discover a non-linear relationship between the immunization campaign parameters that leads to the illness extinction.

The current work is organized as follows: in Sec. II, we present the model and its equilibrium solutions, from which we obtain the $\mathcal{R}_0$ as well as a minimum rate to eradicate the disease. In Sec. III we discuss the effects of constant vaccination in the model. The pulsed vaccination strategy is discussed in Sec. IV, and the implementation of pulsed width in the vaccine campaign is present in Sec. V. Finally, our conclusions are drawn in Sec. VI.

II. MODEL

SEIRS is a compartmental epidemiological model that describes the spread of a given infectious disease in a homogeneously mixed host population, in which individuals are computed into one of the four compartments, namely, susceptible in S, exposed and not yet contagious in E, infectious in I, and recovered in R.[20] The population size ($N = S + E + I + R$) is time-dependent when the natural death rate (μ) is not equal to the birth rate (b). The transition flow between the compartments is schematically represented in Fig. 1. Susceptible individuals become infected through interaction with contagious agents at a rate $\beta I/N$, where β is the transmitting infection rate per interaction. Once a portion of S is infected, it evolves to E, remaining in this compartment by an average time given by $1/\alpha$ (latent period). The parameter α is the rate at which exposed individuals become infectious, migrating to compartment I. Individuals remain in I by an average time $1/\gamma$ (infectious interval), after that they occupy the R compartment, the parameter γ is called recovery rate. In this model, there is no permanent immunity; then, after an average interval $1/\delta$, the individuals in R return to S,[18] in which δ is the immunity loss rate. Furthermore, we consider vaccination of newborns and susceptible.[50] A fraction $p \in [0, 1]$ of newborns are directly immunized, and a portion of S is vaccinated at a rate v with effectiveness $\lambda \in [0, 1]$. The vaccine effect is to
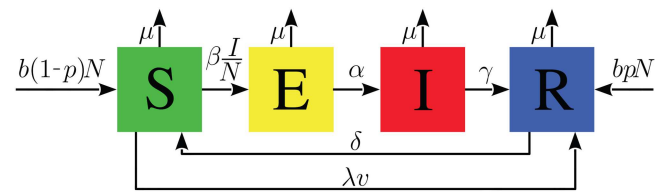

FIG. 1. Schematic representation of the SEIRS model with vaccine inclusion. The compartments (colored boxes), indexed by variables of the system (1), contain fractions of the population at each stage of infection spread. Arrows indicate the flow between them, increase in newborns and loss of population due to death, accompanying the respective transition rates.

give immunity to individuals, transferring, in this model, newborn and susceptible ones to the recovered class. Given the nature of the model, all parameters are non-negative real numbers.

The SEIRS model with vaccination, as described above, is given by the following system of four coupled ordinary differential equations:[50]

$$\frac{dS}{dt} = b(1 - p)N + \delta R - \left(\beta \frac{I}{N} + \lambda v + \mu\right) S,$$

$$\frac{dE}{dt} = \beta \frac{SI}{N} - (\alpha + \mu)E,$$

$$\frac{dI}{dt} = \alpha E - (\gamma + \mu)I,$$

$$\frac{dR}{dt} = bpN + \lambda vS + \gamma I - (\delta + \mu)R. \qquad (1)$$

Other effects also can be considered in this model and incorporated into Eq. (1), such as reaction–diffusion[57] and delay,[58] but this is beyond the present work and will be studied next. Seasonality is included in the model by replacing β by a periodic function,

$$\beta(t) = \beta_0 \left[1 + \beta_1 \cos(\omega t)\right], \qquad (2)$$

where β_0 is the average contagion rate, the seasonality degree is $\beta_1 \in [0, 1]$, and ω is its frequency.[23]

From Eq. (1), the sum of variables followed by a simple manipulation provides us the growth rate of the host population $dN/dt = (b - \mu)N$. Considering this result, the Eq. (1) can be rewritten in a normalized form, without loss of generality, by taking[59]

$$S = Ns, \ E = Ne, \ I = Ni, \text{ and } R = Nr,$$

which gives the respective transformations for the time derivatives of the variables,

$$\frac{ds}{dt} = \frac{1}{N}\left(\frac{dS}{dt} - (b - \mu)S\right),$$

$$\frac{de}{dt} = \frac{1}{N}\left(\frac{dE}{dt} - (b - \mu)E\right),$$

$$\frac{di}{dt} = \frac{1}{N}\left(\frac{dI}{dt} - (b - \mu)I\right),$$

$$\frac{dr}{dt} = \frac{1}{N}\left(\frac{dR}{dt} - (b - \mu)R\right). \qquad (3)$$

This change of variables leads to equations of the same form that would be obtained by assuming $b = \mu$. We get

$$\frac{ds}{dt} = b(1-p) + \delta r - \left[\beta(t)i + \lambda v + b\right]s,$$

$$\frac{de}{dt} = \beta(t)is - (\alpha + b)e,$$

$$\frac{di}{dt} = \alpha e - (\gamma + b)i, \qquad (4)$$

$$\frac{dr}{dt} = bp + \lambda vs + \gamma i - (\delta + b)r,$$

with the constrain $s + e + i + r = 1$. Then, r can be determined in terms of the other three variables, such that we replace it in the first of Eq. (4), reducing the model to the following three-equation system:

$$\frac{ds}{dt} = b(1-p) + \delta - \left[\beta(t)i + \lambda v + \delta + b\right]s - \delta(e + i),$$

$$\frac{de}{dt} = \beta(t)is - (\alpha + b)e, \qquad (5)$$

$$\frac{di}{dt} = \alpha e - (\gamma + b)i.$$

A. Disease-free equilibrium

In general, Eq. (5) is solved numerically. However, for the particular case, when $\beta = \beta_0$ is constant, there are two fixed point solutions, which are DFE and endemic solution.[60] The first one is characterized by the disappearance of the disease in the host population ($i^* = 0$); in the other, the infection remains ($i^* > 0$). First, we investigate the DFE solution given by

$$(s^*, e^*, i^*) = \left(\frac{b(1-p) + \delta}{\lambda v + \delta + b}, 0, 0\right). \qquad (6)$$

This fixed point is stable if all eigenvalues of the Jacobian matrix ($\mathbb{J}$) of the system, computed in DFE, have negative real part.[61] Given the matrix

$$\mathbb{J}_{\text{DFE}} = - \begin{bmatrix} (\lambda v + \delta + b) & \delta & (\beta_0 s^* + \delta) \\ 0 & (\alpha + b) & -\beta_0 s^* \\ 0 & -\alpha & (\gamma + b) \end{bmatrix}, \qquad (7)$$

its eigenvalues are

$$\xi_1 = -(\lambda v + \delta + b), \qquad (8)$$

$$\xi_2 = \frac{-(\alpha + \gamma + 2b) - \sqrt{(\alpha - \gamma)^2 + 4\alpha\beta_0 s^*}}{2}, \qquad (9)$$

$$\xi_3 = \frac{-(\alpha + \gamma + 2b) + \sqrt{(\alpha - \gamma)^2 + 4\alpha\beta_0 s^*}}{2}. \qquad (10)$$

All of them are real numbers, once the constants are positive and $\xi_{1,2}$ are always negative, then the DFE is stable when $\xi_3 < 0$. From this

inequality, we obtain the relation for the stability of this fixed point,

$$\mathcal{R}_0 = \frac{\alpha\beta_0 s^*}{(\alpha + b)(\gamma + b)} < 1. \qquad (11)$$

Therefore, if $\mathcal{R}_0 < 1$, the DFE point is stable, i.e., the disease will die out. On the other hand, if $\mathcal{R}_0 > 1$, the disease will be succeeding in infecting the population.[62] Thus, we establish a stability condition for the DFE relative to the basic reproduction number. The quantity $\mathcal{R}_0$ informs about the evolution of the spread. Note that if $p = \lambda v = 0$, then $s^* = 1$, and we recover the $\mathcal{R}_0$ for the model without vaccine.[24]

Note that Eq. (11) is for the autonomous case, with β and v being constants. However, for periodic diseases without latent period,[63] the $\mathcal{R}_0$ expression can be extended by replacing β_0 with $\langle\beta(t)\rangle$,

$$\langle\beta(t)\rangle = \frac{1}{T_{\text{f}} - T_0} \int_{T_0}^{T_{\text{f}}} \beta(t)dt, \qquad (12)$$

where $T_{\text{f}} - T_0$ corresponds to the seasonality period. In the case studied in this work, we can analyze both the average $\langle\mathcal{R}\rangle$ of the time-dependent reproduction number and its maximum $\mathcal{R}_+$ within a seasonal cycle,[50] being $\langle\mathcal{R}\rangle = \mathcal{R}_0$ and $\mathcal{R}_+ = (1 + \beta_1)\mathcal{R}_0$. Imposing the stable DFE condition on these quantities, we obtain two quotas,

$$\frac{\alpha[b(1-p) + \delta]}{\lambda(\alpha + b)(\gamma + b)}\beta_0 - \frac{(\delta + b)}{\lambda} < v_0, \qquad (13)$$

$$\frac{\alpha[b(1-p) + \delta]}{\lambda(\alpha + b)(\gamma + b)}\beta_0(1 + \beta_1) - \frac{(\delta + b)}{\lambda} < v_+. \qquad (14)$$

The disease extinction is guaranteed when the relationship $v_+ \leq v$ is verified. However, this upper limit for the vaccination rate can be greater than enough, with $v_0 \leq v$ being sufficient to reach the DFE in our simulations. Note that this threshold is the same in the autonomous case. As a numerical example, considering $\lambda = 1$, $p = 0.25$ $b = 0.02$, $\beta_0 = 270$, $\delta = 0.25$, $\alpha = 100$, and $\gamma = 100$, we obtain a quota $v_0 = 0.445$. Therefore, for a constant vaccination campaign, the minimum rate is 44.5% of vaccinated susceptible. A value very close to those numerically obtained in Sec. III and annual vaccination rates in Secs. IV and V.

B. Endemic equilibrium

Considering the autonomous case, the endemic equilibrium point EE $(\widetilde{s}, \widetilde{e}, \widetilde{i})$ is given in terms of $\mathcal{R}_0$ and s^* as

$$\widetilde{s} = \frac{(\alpha + b)(\gamma + b)}{\alpha\beta_0} = \frac{s^*}{\mathcal{R}_0}, \qquad (15)$$

$$\widetilde{e} = \frac{(\gamma + b)[b(1-p) + \delta]}{\alpha\beta_0 s^* + \delta(\alpha + \gamma + b)\mathcal{R}_0}(\mathcal{R}_0 - 1), \qquad (16)$$

$$\widetilde{i} = \frac{\alpha[b(1-p) + \delta]}{\alpha\beta_0 s^* + \delta(\alpha + \gamma + b)\mathcal{R}_0}(\mathcal{R}_0 - 1). \qquad (17)$$

In this solution, the disease is permanent in the host population. It is worth to note that for the inverse relation $\widetilde{s}$ proportional to $\mathcal{R}_0^{-1}$, the

scenario without vaccination verifies the result[24] $\widetilde{s} = \mathcal{R}_0^{-1}$. This fixed point exists only if $\mathcal{R}_0 > 1$ since $\mathcal{R}_0 < 1$ implies $\widetilde{e}, \widetilde{i} < 0$ in Eqs. (16) and (17). It means that in the case of stable DFE, there is no endemic fixed point, recovering the information previously discussed.

As in the DFE case, we analyze the stability of the EE fixed point through eigenvalues of the Jacobian matrix $\mathbb{J}_{EE}$ computed on it, being

$$\mathbb{J}_{EE} = - \begin{bmatrix} (\beta_0\widetilde{i} + \lambda v + \delta + b) & \delta & (\beta_0\widetilde{s} + \delta) \\ -\beta_0\widetilde{i} & (\alpha + b) & -\beta_0\widetilde{s} \\ 0 & -\alpha & (\gamma + b) \end{bmatrix}. \quad (18)$$

The correspondent characteristic polynomial is given by

$$\mathcal{P}(\zeta) = \zeta^3 + c_2\zeta^2 + c_1\zeta + c_0, \quad (19)$$

where the coefficients are

$$c_0 = (\beta_0\widetilde{i} + \lambda v + \delta + b)\left[(\alpha + b)(\gamma + b) - \alpha\beta_0\widetilde{s}\right] + \beta_0\widetilde{i}\left[\alpha(\beta_0\widetilde{s} + \delta) + \delta(\gamma + b)\right], \quad (20)$$

$$c_1 = (\beta_0\widetilde{i} + \lambda v + \delta + b)(\alpha + \gamma + 2b) + (\alpha + b)(\gamma + b) + \beta_0(\delta\widetilde{i} - \alpha\widetilde{s}), \quad (21)$$

$$c_2 = \beta_0\widetilde{i} + \lambda v + \alpha + \gamma + \delta + 3b. \quad (22)$$

Having such coefficients and using the Routh–Hurwitz criterion,[64] it is possible to find a parametric relationship for the EE point stability. In this way, the real part of the all three eigenvalues is less than zero if and only if

$$c_0, c_1, c_2 > 0; \text{ and } c_0 < c_1 c_2. \quad (23)$$

Fulfilled the above conditions, once the EE point exists, it is attractive.[70] In the context of the present work, we verify that the EE point is asymptotically stable for the parameters used in our simulations, as already described in Sec. II A: $\lambda = 1$, $p = 0.25$, $b = 0.02$, $\delta = 0.25$, $\alpha = 100$, $\gamma = 100$, $\beta_0 = 270$, and $v \in [0, v_0 = 0.445)$, where $\mathcal{R}_0 > 1$.

For the non-autonomous system, where $\beta = \beta(t)$ is the periodic function given in Eq. (2), the DFE solution is the only one of the fixed-point type. In other words, the fixed point solution with $i \neq 0$ does not exist when the transmissivity is an explicit function of time. In this case, endemic solutions are not fixed points but consist of orbits that can be periodic or chaotic. Figure 2 shows the system evolution from the initial condition $P_0(s_0, e_0, i_0) = (0.39, 0.0039, 0.0039)$ in the two cases: (1) autonomous (with $\beta_1 = 0$), where the trajectory (orange line) spirals to the attractive fixed point EE $(\widetilde{s}, \widetilde{e}, \widetilde{i}) \approx (0.371, 0.001, 0.001)$; (2) non-autonomous system (with $\beta_1 = 0.28$), where the trajectory (light-blue line) evolves during a transient time around EE point and converges to the periodic attractor (blue line). To obtain these curves, we adopt the aforementioned parametric configuration and consider a constant vaccination rate $v = 0.17$. In Secs. III– VI, we numerically investigate the impacts of different vaccination protocols on the dynamics of Eq. (5) with seasonality, focusing on the infected population.
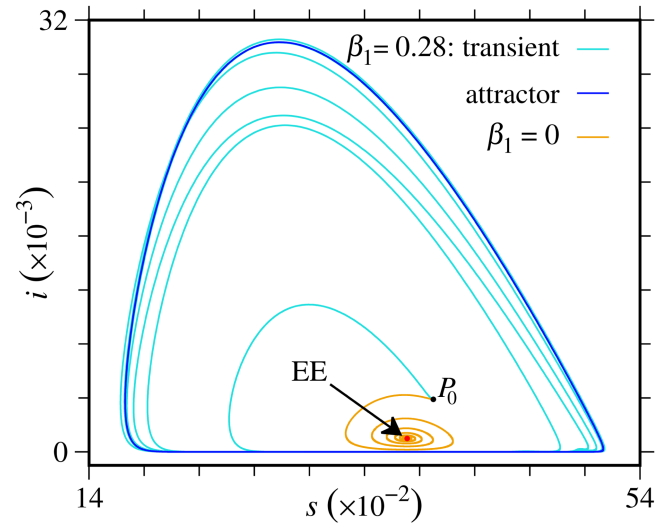

FIG. 2. Trajectories evolving from the initial condition $P_0(s_0, e_0, i_0) = (0.39, 0.0039, 0.0039)$ (black dot). We consider the parameters: $v = 0.17$, $\lambda = 1$, $p = 0.25$, $b = 0.02$, $\beta_0 = 270$, $\delta = 0.25$, $\alpha = 100$, and $\gamma = 100$. For $\beta_1 = 0$, the trajectory (orange line) spirals toward the attractive fixed point EE(0.371, 0.001, 0.001) (red dot). In the non-autonomous case ($\beta_1 = 0.28$ and $\omega = 2\pi$), the system evolves (light-blue line) around the point EE converging to the periodic attractor (blue line).

III. CONSTANT VACCINATION STRATEGY

Continuous vaccination campaign is modelled by a constant vaccine term v in Eq. (5), which represents a fraction of the host population being vaccinated at every time step. This approach can be used for modelled mass vaccination programs.[55] In this campaign, a certain amount of the population is vaccinated in a short period of time. Some examples are the mass campaign against measles,[65] smallpox,[66] and COVID-19.[67] In this case, p is also constant. To numerically integrate the system of differential equations, we use the fourth-order Runge–Kutta method[68] with a fixed step of 10^{-3}. It is important to mention that without spoiling the analyses, we consider the vaccine effectiveness $\lambda = 1$. Even so, this term can be understood, more generally, as absorbed by v, since these always appear as a product, maintaining the equations form.

Figure 3 displays three different numerical solutions to Eq. (5) for different p and v. In these results, we consider $b = 0.02$, $\beta_0 = 800$, $\beta_1 = 0.20$, $\delta = 0.25$, $\alpha = 40$, $\gamma = 100$, and $\omega = 2\pi$. In this work, the time unity is years. In order to interpret these values, we consider b as an annual birth rate, with the other four rates being annual too. Thus, $\omega = 2\pi$ means seasonality with a period of one year. Regarding the vaccination parameters, the reference curve (red line) is obtained for $p = v = 0$; for the other two, $p = 0.25$ and $v = 0.2$ for the blue curve and $v = 0.4$ for the green one. We adopt the initial condition $(s_0, e_0, i_0) = (0.9, 0, 0.1)$ and discard the first 10^5 integration steps as transient. For these configurations, the solutions of the system are limit cycles, which are projected onto the plane $i \times s$ in Fig. 3(a). These cycles contract as the vaccination rate increases, with a significant decrease in the local maxima of curve i,
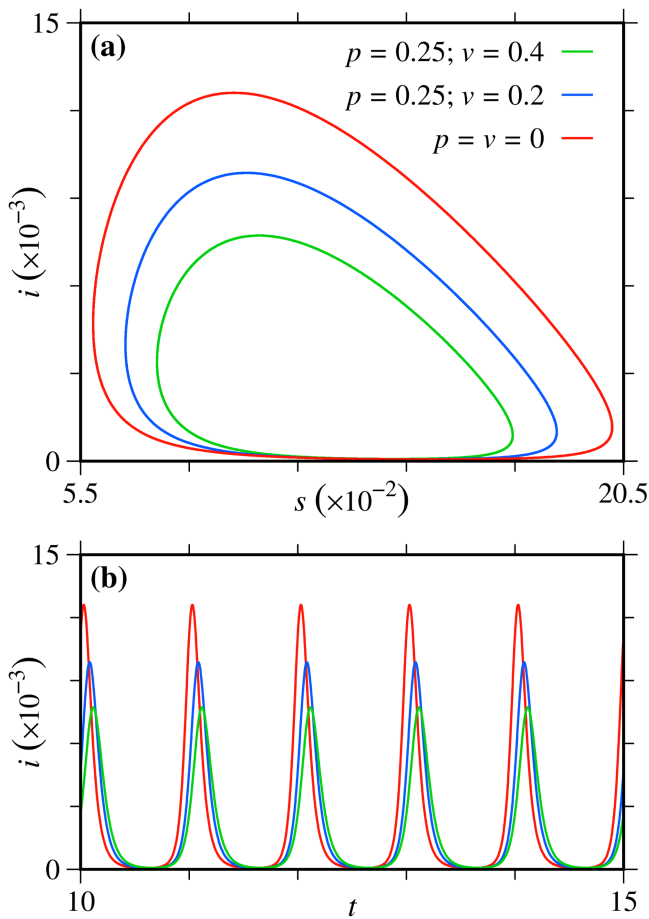
FIG. 3. Numerical solutions to Eq. (5) for three different values of p and v. (a) Limit cycles obtained for $p = v = 0$ (red curve) and $p = 0.25$, with $v = 0.2$ (blue curve) and $v = 0.4$ (green curve). (b) Time series for i corresponding to the limit cycles in the same colors according to the legend. We consider $b = 0.02$, $\beta_0 = 800$, $\beta_1 = 0.20$, $\delta = 0.25$, $\alpha = 40$, $\gamma = 100$, $\omega = 2\pi$, and initial condition $(s_0, e_0, i_0) = (0.9, 0, 0.1)$. We discard 10^5 integration steps as transient.

as shown in Fig. 3(b). We find that the presence of a vaccine campaign causes a reduction in the maximum number of infects at a time, and this effect is amplified with the v increment. Compared to the reference curve, a constant vaccination rate of one-quarter of the newborn population and one-fifth of the susceptible ones, for year, leads to approximately a 21.4% reduction in peak infections. Intensifying vaccination to a rate of 40% of the susceptible population per year, this reduction reaches $\approx 38.9\%$.

For the next numerical simulations, based on the Gabrick's work,[24] we consider the parameters $b = 0.02$, $\beta_0 = 270$, $\beta_1 = 0.28$, $\delta = 0.25$, $\alpha = 100$, $\gamma = 100$, and $\omega = 2\pi$. To compute the impact of the vaccine on the system, over a given finite time interval, we consider the ratio

$$\theta = \frac{A_v}{A_0}, \tag{24}$$

where A_v and A_0 are the areas under the i curve with and without vaccine, respectively. Being

$$A_v = \int_{t_0}^{t_0 + \Delta t} i(t)dt, \tag{25}$$

$$A_0 = \int_{t_0}^{t_0 + \Delta t} i(t; p = v = 0)dt, \tag{26}$$

where A_0 is the reference value. From this relation, we conclude that if $\theta < 1$, then the vaccination campaign reduces the total number of infected individuals, and if $\theta > 1$, the campaign has the undesired effect of increasing it. $\theta = 1$ means that the vaccination has no effect on the total infections over time.

Figure 4 shows the influence of vaccination in two different strategies. In panel (a), we fixed the fraction of newborns $p = 0.25$ and get θ as a function of the vaccination rate $v \in [0, 1]$, with the horizontal axis discredited in steps of $\Delta v = 10^{-2}$. We evolve the system from the same initial condition used in Fig. 3 and calculate θ both for the first 75 years without transient discard (black curve) and, past 100 years of evolution, for the last 75 years (blue curve). Without discarding the early years, θ presents a linear decay as a function of v, increasing until $v \approx 0.44$ and stabilizing in $\theta \approx 0.075$. This value is due to the nonzero area associated with the spread of infection from the initial condition. In the blue curve, we see that the DFE is reached for $v \geq 0.44$ (gray background). Furthermore, it is worth to mention that in our simulation if we consider a large number of years, e.g., 100 and 125 years, the DFE also is reached for $v \geq 0.44$. Figure 4(b) displays θ as a function of p, with $v = 0.1$. This result shows when whole newborns are vaccinated, a reduction of $\approx 12.5\%$ of the total infected individuals occurs.

We evaluate the effects of combining different newborns and susceptible vaccination rates in the parameter plane $p \times v$, with θ being in color scale, as displayed in Fig. 5. Our results show the prevalence of v over p in reducing the spread of infection. This is due to the intrinsic characteristics of the model; if δ decreases, the parameter p becomes more relevant. DFE is achieved within 75 years from the onset of infection by (v, p) pairs from the dashed white line to the right of it, defined by the straight line equation $c_1 : p + 18.55v - 8.22 = 0$. Extinction of infection in the host population occurs when $e = i = 0$ and can be verified in simulations with a given numerical precision. In order to determine the boundary line c_1 more accurately, we integrate the system in the region defined by $v \in [0.39, 0.46]$ and $p \in [0, 1]$ in a uniform grid of 201×201 points. Still in Fig. 5, the blue band indicates that the constant vaccination strategy leads to a significant reduction in the total infections, computed around 20% of the reference. In the green band, where $v \approx 0.2$, the reduction is around 50%. For small vaccination rates, with $v \approx 10\%$ and less, the amount of infections decreases only slightly, being around 70% to 80% (gradient from orange to red) of the result without vaccination, even larger than 90% (magenta band).

The vaccination does not only affects the number of infected individuals but also the dynamics. Such effects are examined by hysteresis-type bifurcation diagrams (HTBDs), as shown in Fig. 6.
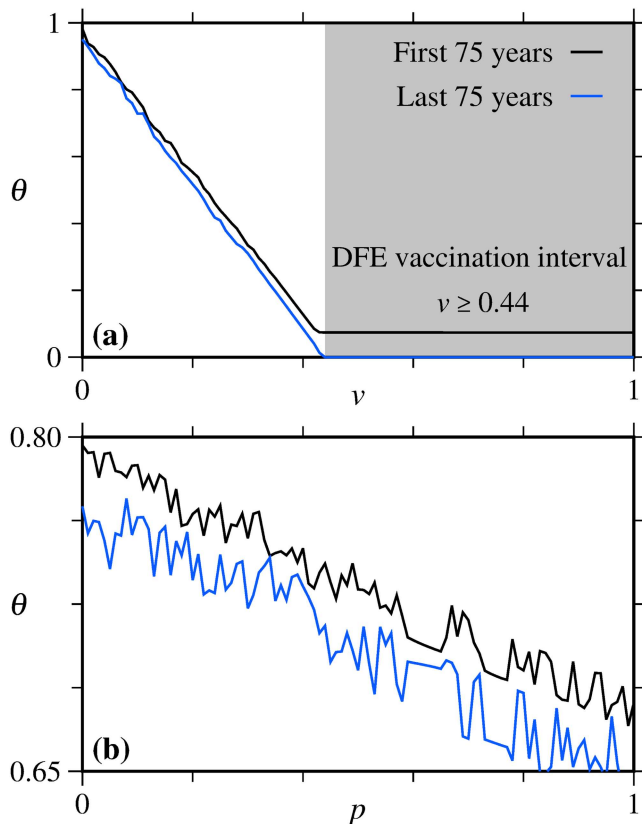
FIG. 4. (a) θ as a function of rate v with $p = 0.25$. DFE is reached for $v = 0.44$ (gray background). (b) θ as a function of newborn vaccine p with $v = 0.1$. Vaccination of newborns reduced $\approx 12.5\%$ the total of infected individuals. Horizontal axis discredited in steps of 10^{-2}. Results of the first 75 years without transient discard (black curve) and evaluated the last 75 years (blue curve) after 100 years of the system evolution. We consider $b = 0.02$, $\beta_0 = 270$, $\beta_1 = 0.28$, $\delta = 0.25$, $\alpha = 100$, $\gamma = 100$, and $\omega = 2\pi$; initial condition $(s_0, e_0, i_0) = (0.9, 0, 0.1)$.

This kind of bifurcation diagram is generated by evolving the system in a given discretized interval of a control parameter in both directions along the horizontal axis, first in its growth (red points) and then in decrease (blue points), assuming the final state of the system at the current parameter value as the initial condition for the next one. This numerical technique is especially useful for finding bi-stability, when it exists.[69] Figure 6(a) displays a HTBD of i local maxima values ($i_{\max}$) as a function of the susceptible vaccination rate. To compute the peaks in the i time series, we discard the first 10^5 integration steps as transient and evaluate the evolution of the infection over the last 75 years in the simulation. For the considered parameters, the bi-stability dynamics between chaotic and periodic attractors exist without vaccination.[24] The inclusion of vaccination is able to destroy the bi-stability for some parameter values. However, the bi-stability remains in two ranges of the control parameter, highlighted in Fig. 6(a), by the gray and green background columns. In the approximate interval $v \in (0.155, 0.165)$ (gray background) the periodic orbit (blue dots) has a maximum value $i_{\max} \approx 0.032$,
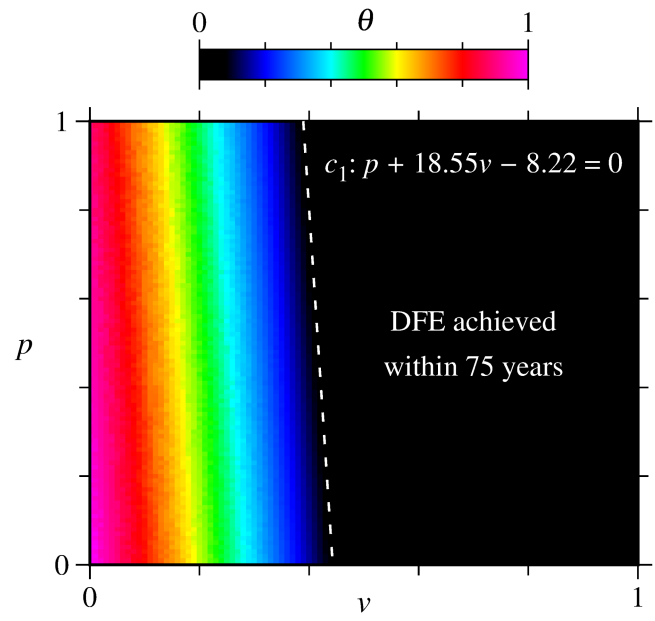

FIG. 5. Parameter plane $p \times v$ with θ in color scale. Both axes discretized in steps of 10^{-2}. We consider $b = 0.02$, $\beta_0 = 270$, $\beta_1 = 0.28$, $\delta = 0.25$, $\alpha = 100$, $\gamma = 100$, and $\omega = 2\pi$. θ is calculated for the first 75 years of infection, without transient discard and with initial condition $(s_0, e_0, i_0) = (0.9, 0, 0.1)$. DFE occurs from the dashed white line (c_1) to the right of it, where $p \geq 8.22 - 18.55v$.

while the chaotic one (red dots) has a smaller maximum of $i_{\max} \approx 0.026$. Also in the interval $v \in (0.256, 0.263)$ (green background), we observe the periodic orbit with an extreme value of $i_{\max}$ slightly higher than that seen from the chaotic one. Chaotic behavior can be related to non-predictability in infectious diseases spread.[24] Prior knowledge of these behaviors or how they can be modified is crucial for epidemic control strategies. Figures 6(b) and 6(c) display the $i \times s$ projection of the attractors obtained for the highlighted values in the bi-stability for, respectively, $v = 0.16$ and $v = 0.26$. Both plots show the periodic solution (blue line) with a higher peak than the chaotic one (red line). For $v = 0.16$, we observe a chaotic attractor from the initial condition $P_1(s_0, e_0, i_0) = (0.9, 0, 0.1)$, while the periodic one emerges for $P_2(s_0, e_0, i_0) = (0.3, 0.03, 0.03)$. However, for $v = 0.26$, P_1 leads to the periodic attractor and P_2 to the chaotic one. The magnification in the panel (c) exhibits a small amplitude local maximum of i, occurring before the large increase in infectious cases and showing the two maxima as obtained in the bifurcation diagram.

IV. PULSED VACCINATION STRATEGY

Periodic vaccination consists of the appliance of vaccine in a certain fraction of the population in periodic time intervals. Examples of this strategy is considered in seasonal influenza[56] and in control of childhood viral infections, such as measles and polio.[53] In our modeling approach, we consider this immunization strategy that consists of maintaining a minimum level $v = v_{\min}$ during
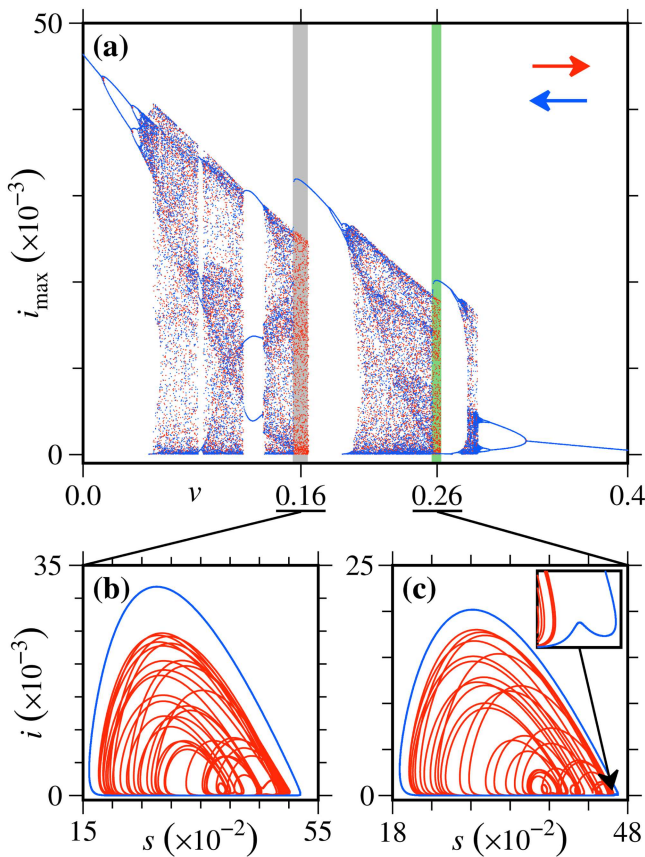
FIG. 7. Schematic illustration of pulsed v with maximum v_{max} (dashed gray line level) and minimum level v_{min} (solid gray line). Pulses in four different timings relative to $\beta(t)$ (black curve): at inflections (green and magenta vertical lines) and at the local minimum and maximum, blue and red lines, respectively.

FIG. 6. (a) Hysteresis type bifurcations diagram (HTBD) for i local maxima values (i_{max}) as function of $v \in [0, 0.4]$ discretized in steps of 4×10^{-4}. We consider $b = 0.02$, $\beta_0 = 270$, $\beta_1 = 0.28$, $\delta = 0.25$, $\alpha = 100$, $\gamma = 100$, $\omega = 2\pi$, and $p = 0.25$. For each value of v, a transient of 10^5 integration steps is discarded and computed i_{max} over the last 75 years of the infection. The red points are in the forward v direction and blue points in the backward direction. Gray and green backgrounds highlight bi-stability intervals. Projections in the plane $i \times s$ of periodic (blue line) and chaotic (red line) attractors coexisting for (b) $v = 0.16$ and (c) $v = 0.26$.

the year and raising the vaccination rate to $v = v_{max} \geq v_{min}$ in concentrated pulses at specific times according to the oscillation of the transmissivity. An illustrative scheme is shown in Fig. 7, where different pulse timings are superimposed on the periodic curve $\beta(t)$ (black line). We consider four variants of the same strategy, in which the pulse occurs, relative to the $\beta(t)$, at every time corresponding to the inflection point at decreasing (green line), local minimum (blue line), inflection point at the curve growth (magenta line), and local maximum (red line). Being the vaccination rate,

$$v(t; \tau) = \begin{cases} v_{max}, & \text{if } \{t - \tau\} = 0, \\ v_{min}, & \text{otherwise,} \end{cases} \qquad (27)$$
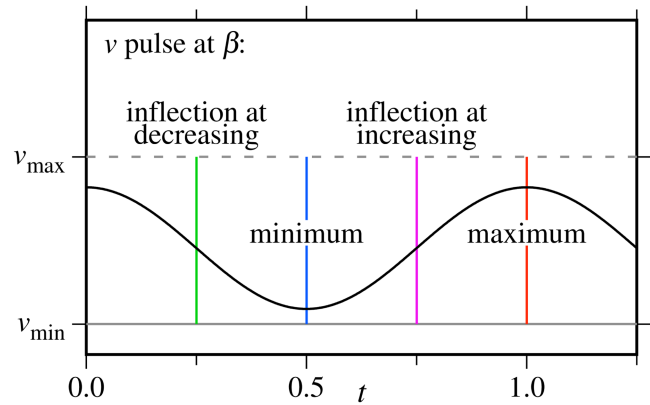
where $\{t - \tau\}$ is the non-integer part of $(t - \tau)$. For the first variant of the strategy, we have $\tau = 0.25$, in the second $\tau = 0.5$, next $\tau = 0.75$, and in the last one $\tau = 0$.

Considering a time interval of $\approx 9\,\text{h}$ in one day per year, we investigate the impact on total infected in the first 75 years of infection, with $v_{min} = 0$ and $v_{max} \in [0, 1000]$, where $v = 1000$ means that the entire susceptible population is vaccinated in one pulse since the integration step is 10^{-3} and the proportion of people vaccinated is given by the product of the campaign duration with the vaccination rate. Furthermore, we adopt $p = 0$ and the same initial condition used in Sec. III.

Figure 8 displays θ as a function of v_{max}, with the horizontal axis discretized in steps of $\Delta v_{max} = 1$, equivalent to increments of 0.1% in the reach of the immunization campaign. The four variants of the strategy are covered, with the pulse applied at the first (green) and second (magenta) inflections of $\beta(t)$ and, complementary, for both $\tau = 0.5$ (blue) and $\tau = 0$ (red), at times corresponding to the transmissivity minimum and maximum, respectively. These results are practically the same. There is no expressive difference as to when a concentrated immunisation campaign works, with a slight advantage in applying the pulse at the local maximum ($\tau = 0$) or second inflection ($\tau = 0.75$) of the transmissivity curve. When the campaign coincides with the extremes of the $\beta(t)$ curve ($\tau = 0$ and $\tau = 0.5$), DFE is achieved within the initial 75 years (gray background) from $v_{max} = 452$, i.e., vaccinating from 45.2% of the susceptible population on a single day per year. This threshold is 49.0% for $\tau = 0.25$ and 44.4% for $\tau = 0.75$, the latter being the best result.

According to our simulations, considering a not null baseline $v_{min} > 0$, it is possible to reduce the pulse amplitude and yet result in the extinction of the disease in the host population within 75 years. In Fig. 9, we show the parameter plane $v_{max} \times v_{min}$ reinforcing this proposal. We define $\tau = 0.75$, applying the pulse at the moment of inflection during the increase of the transmissivity, varying $v_{min} \in [0, 0.4]$ and $v_{max} \in [100, 400]$ in a uniform grid of 101×101 points. We highlight the white dashed line $c_2 : v_{max} + 1000 v_{min} - 444 = 0$, from which we obtain DFE. Pairs (v_{min}, v_{min}) in the blue
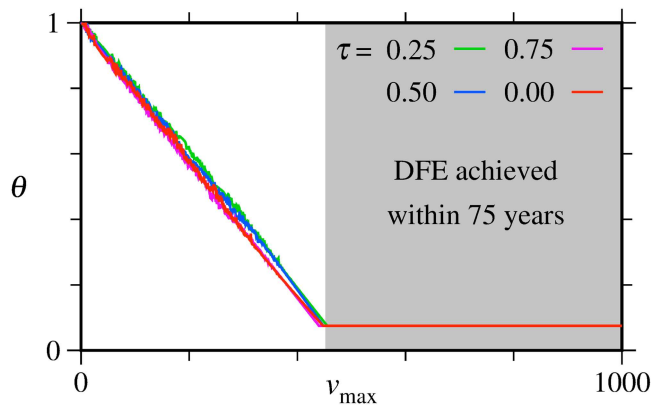
FIG. 8. θ as a function of $v_{max} \in [0, 1000]$ from four variants of the pulsed vaccination strategy and obtained in the first 75 years of infection. Horizontal axis discretized in 1001 equidistant points. We consider $b = 0.02$, $\beta_0 = 270$, $\beta_1 = 0.28$, $\delta = 0.25$, $\alpha = 100$, $\gamma = 100$, $\omega = 2\pi$, and $p = v_{min} = 0$. Initial condition $(s_0, e_0, i_0) = (0.9, 0, 0.1)$. Pulse application timing identified in colors, according to the legend. DFE is achieved (gray background) within 75 years for $v_{max} \geq 452$ with $\tau \in \{0, 0.5\}$, $v_{max} \geq 459$ for $\tau = 0.25$, and $v_{max} \geq 444$ when $\tau = 0.75$.

band bring the total infected to $\approx 20\%$ of those that would occur without vaccination, e.g., how we get with the base rate $v_{min} \approx 0.28$ and the intensive campaign $v_{max} = 100$, the latter meaning vaccination of 10% of the susceptible population. Since the base value throughout the year is around $v_{min} = 0.125$, even with $v_{max} = 100$, the number of people infected during the 75 years simulated is reduced by approximately half (green band), when compared to the reference case.

Along lines parallel to c_2, the proportion of susceptible vaccinated annually is a constant given by

$$\rho_{line} = 0.001 v_{max} + v_{min}. \tag{28}$$

Thus, on line c_2, we have $\rho_{c_2} = 0.444$, close to the DFE threshold value in line c_1 with $p = 0$, as shown in Sec. III. In these simulations, an immunization campaign that reaches $\approx 22.5\%$ of susceptible annually reduces to 50% of the accumulated of infected people, whereas a rate of $\approx 38\%$ causes a decrease of 80%. Similar values to those obtained with v constant and without newborns vaccination, as displayed in Fig. 5. The strategy of intensifying immunization in pulses allows the reduction at baseline, being v_{min} less than the rates required for the same results with constant vaccination rate.

V. PULSED WIDTH VACCINATION STRATEGY

Extending the proposal of Sec. IV, we modify the pulsed vaccination strategy considering, now, a longer duration of the intensified campaign. Similarly to the formulation of Eq. (26), the pulse is centered at $t = \tau + k, \forall k \in \mathbb{Z}$, but with a width of $D \in [0, 1]$, which corresponds to the duty cycle. Outside the intensive campaign interval, vaccination assumes a baseline rate v_{min}, according to the following
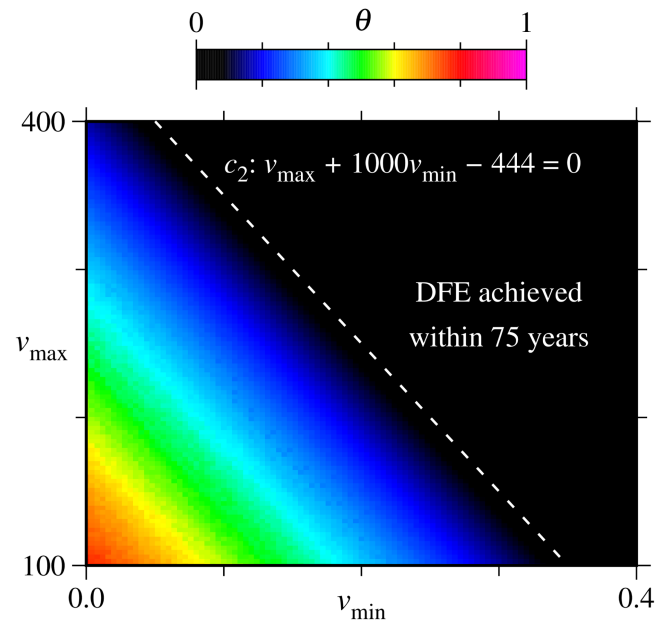

FIG. 9. Parameter plane $v_{max} \times v_{min}$ discretized on a uniform grid of 101×101 points, with θ (color scale) calculated for the first 75 years of infection. We consider $b = 0.02$, $\beta_0 = 270$, $\beta_1 = 0.28$, $\delta = 0.25$, $\alpha = 100$, $\gamma = 100$, $\omega = 2\pi$, $p = 0$, and $\tau = 0.75$. Initial condition $(s_0, e_0, i_0) = (0.9, 0, 0.1)$. DFE occurs from the dashed white line (c_2) to the right of it, where $v_{max} \geq 444 - 1000 v_{min}$.

mathematical description:

$$v(t; \tau) = \begin{cases} v_{max}, & \text{if } \left\{(t - \tau) + \dfrac{D}{2}\right\} \leq D, \\ v_{min}, & \text{otherwise.} \end{cases} \tag{29}$$

Remembering that $\{x\} \in [0, 1)$ is the non-integer part of the real number x. Figure 10 displays a schematic illustration of this strategy, where the seasonal transmissivity (black curve) is superimposed on the time-dependent vaccination rate curve (magenta curve). For instance, the value $D = 0.2$ corresponds to 1/5 of one year. The concentrated pulse strategy, according Eq. (26), is recovered when $D = 0$. As for $D = 1$, we return to the constant vaccination rate. Based on the best result presented in Sec. IV, in the next simulations, we adopt $\tau = 0.75$.

First, we keep $p = 0$ and obtain θ in the parameter planes as shown in Fig. 11. As in Secs. I–IV, we take into account the first 75 years of infection and consider the same initial condition. Both panels display uniform grids of 101×101 points.

We analyze the results taking into account the annual reaching of the immunization campaign, which is given by

$$\rho = v_{min} + D(v_{max} - v_{min}), \tag{30}$$

and the proportion of vaccinated susceptible during each pulse, that is,

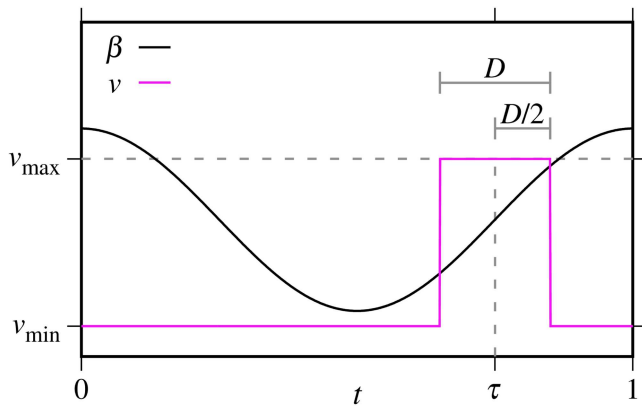$$\rho_{pulse} = D v_{max}. \tag{31}$$

FIG. 10. Schematic illustration of pulsed width vaccination. Transmissivity $\beta(t)$ (black curve) superimposed by vaccination rate $v(t)$ (magenta curve), it is on two levels: maximum v_{max} (dashed gray line level) and minimum v_{min}. Pulse width D centered on τ, which is a time instant relative to the seasonal cycle.

In Fig. 11(a), we fix the baseline $v_{min} = 0$ and vary the two remaining parameters of Eq. (28) in the range $0 \leq D, v_{max} \leq 1$. In this configuration $\rho = \rho_{pulse}$ and the DFE threshold is obtained from $\rho_{pulse} = 0.44$, i.e., from the curve $c_3 : Dv_{max} = 0.44$ to the right of it. Already $\rho_{pulse} = 0.28$ leads to $\theta \approx 0.4$ (cyan band), value obtained along the curve $c_4 : Dv_{max} = 0.28$ (dashed black line). Similar relationships can be obtained for the other θ values, with the balance between pulse height and duty cycle being the determining characteristic for reducing the number of infected people over the 75 years simulated. Figure 11(b) illustrates the parameter plane $v_{min} \times D$ with $v_{max} = 0.5$, where we evaluate the baseline vaccination interval $0 \leq v_{min} \leq 0.4$. As evidenced in panel (a), the constant θ curves are determined by the proportion of susceptible individuals vaccinated during a year, so we get them from Eq. (29). We check that DFE is reached from the curve $c_5 : (0.44 - 0.5D)/(1 - D)$ to the right, where 44% of susceptible are vaccinated annually. The total infected are reduced to $\approx 40\%$ around the curve $c_6 : (0.28 - 0.5D)/(1 - D)$ (black dashed line), being 28% of susceptible vaccinated along each year.

Inclusion of newborns immunization changes the minimum proportion of susceptible immunized annually that leads to DFE. In order to obtain the boundary surface c_{DFE} as a function of p, we use the equation of the line c_1, as described in Sec. III. Assuming a constant vaccination rate $v = \rho_{DFE}$ along that line and relating to Eq. (29), we infer

$$v_{min} + D(v_{max} - v_{min}) - \frac{8.22 - p}{18.55} = 0. \quad (32)$$

DFE is achieved, during the simulated 75 years, once

$$v_{min} + D(v_{max} - v_{min}) \geq \frac{8.22 - p}{18.55}. \quad (33)$$

This relation recovers the equations obtained for the thresholds c_1, c_2, c_3, and c_5 presented throughout the text. Note that in the plane, c_{DFE} reduces to curves.

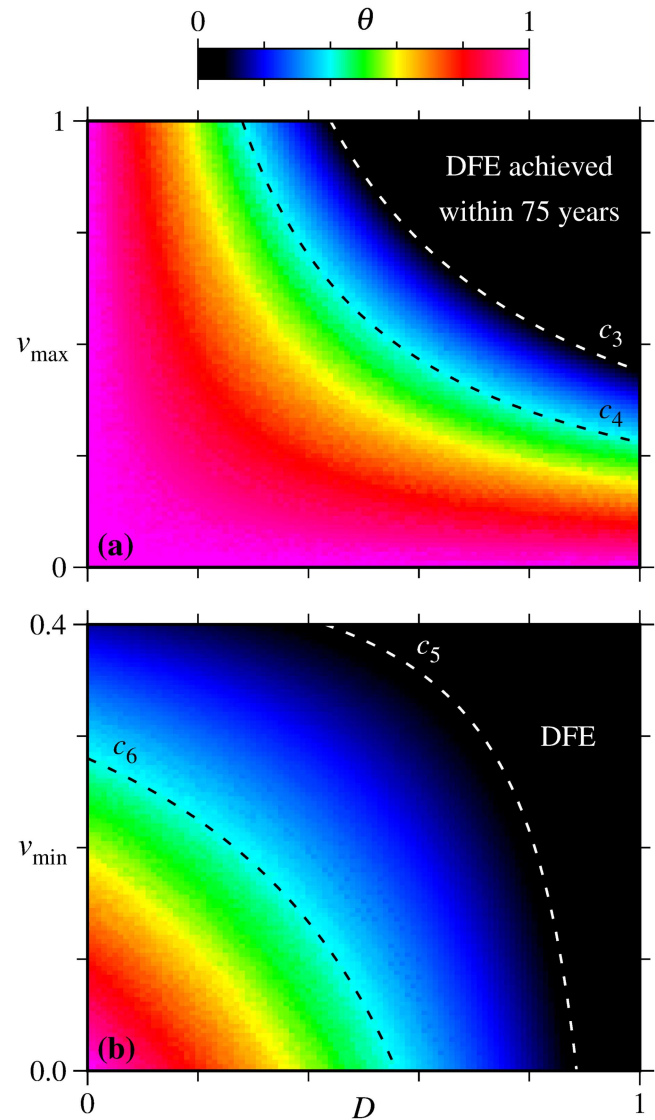In addition, the bi-stability depends on the pulsed vaccination

FIG. 11. Parameter planes discretized on a uniform grid of 101×101 points, with θ (color scale) calculated for the first 75 years of infection. (a) Plane $v_{max} \times D$ with $v_{min} = 0$ fixed. DFE threshold $c_3 : Dv_{max} = 0.44$ and $\theta \approx 0.4$ along the curve $c_4 : Dv_{max} = 0.28$ (black dashed line). (b) Plane $v_{min} \times D$ with $v_{max} = 0.5$ fixed. DFE threshold $c_5 : v_{min} = (0.44 - 0.5D)/(1 - D)$ and $\theta \approx 0.4$ along the curve $c_6 : v_{min} = (0.28 - 0.5D)/(1 - D)$ (black dashed line). We consider $b = 0.02$, $\beta_0 = 270$, $\beta_1 = 0.28$, $\delta = 0.25$, $\alpha = 100$, $\gamma = 100$, $\omega = 2\pi$, $p = 0$, and $\tau = 0.75$. Initial condition $(s_0, e_0, i_0) = (0.9, 0, 0.1)$. In both panels, DFE occurs from the dashed white lines (c_3 and c_5) to the right, where $\rho \geq 0.44$.

parameters. Figure 12(a) displays a HTBD of infected local maxima values (i_{max}) as a function of $v_{max} \in [0, 1]$, with $p = v_{min} = 0$ and $D = 0.4$. The results yielded in forward direction are red points and backward ones are the blue points. The peaks are computed discarding the first 10^5 integration steps as transient and evaluate
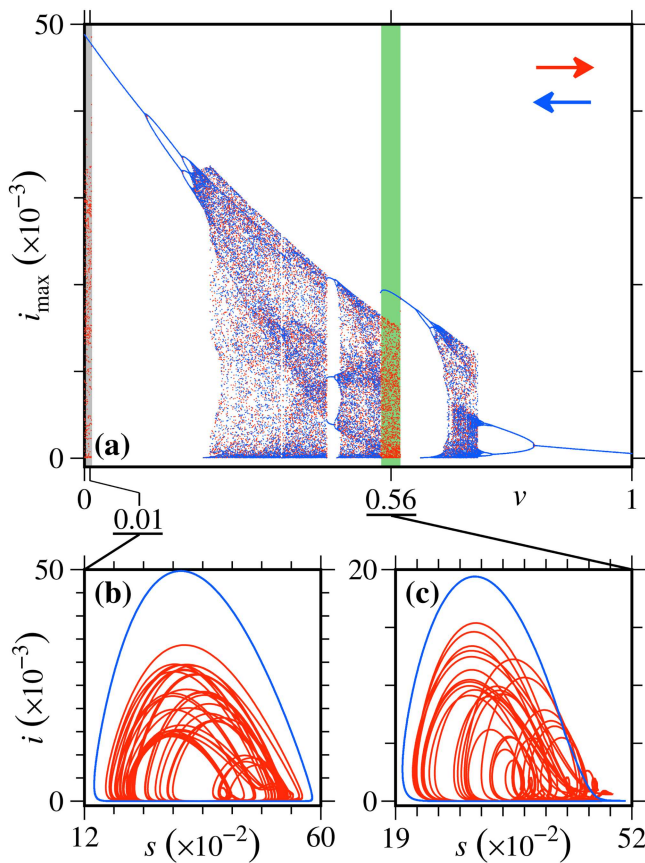
FIG. 12. (a) Hysteresis type bifurcations diagram (HTBD) for i local maxima values (i_{max}) as function of $v_{max} \in [0, 1]$ discretized in steps of 10^{-3}. We consider $b = 0.02$, $\beta_0 = 270$, $\beta_1 = 0.28$, $\delta = 0.25$, $\alpha = 100$, $\gamma = 100$, $\omega = 2\pi$, $p = v_{min} = 0$, and $D = 0.4$. For each value of v_{max}, a transient of 10^5 integration steps is discarded and computed i_{max} over the last 75 years of the infection. Red points are in the forward v_{max} direction and blue ones in the backward direction. Gray and green backgrounds highlight bi-stability intervals. Projections in the plane $i \times s$ of periodic (blue line) and chaotic (red line) attractors coexisting for (b) $v = 0.01$ and (c) $v = 0.56$.

the i series over the last 75 years in the simulation. Similarly to the case of a constant vaccination rate, as shown in Fig. 6(a), there are two ranges (highlighted backgrounds) of the control parameter where periodic and chaotic orbits coexist. For $v_{max} \in [0, 0.014)$ (gray background), the periodic orbit (blue dots) has a maximum value $i_{max} \approx 0.049$, However, the chaotic one (red dots) has a smaller maximum of $i_{max} \approx 0.036$, as also showed by the attractors projection in Fig. 12(b) for $v_{max} = 0.01$. In the next interval $v_{max} \in (0.542, 0.577)$ (green background), the periodic orbit presents a maximum value $i_{max} \approx 0.019$, while the chaotic one has an extreme ≈ 0.015, i.e., the periodic solution has peak infection values of 26.7% above the chaotic case. This difference between the peak of infectious is better observed in the $i \times s$ projection of the attractors, as displayed in Fig. 12(c), for $v_{max} = 0.56$. The chaotic solutions (red line) in both Figs. 12(b) and 12(c) are obtained from the initial condition

P_1, and the periodic attractors (blue line) are from (b) $P_3(s_0, e_0, i_0)$ = (0.27, 0.05, 0.05) and (c) $P_4(s_0, e_0, i_0)$ = (0.28, 0.02, 0.02).

VI. CONCLUSIONS

In this work, we study an SEIRS model with seasonal transmissivity and vaccination control. Considering an autonomous version of the system, we obtain two equilibrium points: the DFE and the endemic fixed point. For the DFE, we established a limit for the vaccination rate as function of the other parameters in the model. We find that the endemic solution can only exist if the DFE is not stable. By numerical simulations, we explore three different vaccination strategies in the non-autonomous case: constant, pulsed, and pulsed width vaccination strategy. All are based on immunizing a proportion of susceptible individuals as well as a fraction of newborns. In order to evaluate these three different strategies, we analyze the accumulated infected over a simulated interval of 75 years:

(i) The first one refers to a constant vaccination rate applied to the susceptible individuals. Our results show that the immunization of newborns is able to slightly reduce the total number of infected in the simulated time interval. However, vaccination of susceptible is more efficient, with a constant rate of $\approx 44\%$, or greater, leading to the extinction of the infection in the host population. We also identify the occurrence of bi-stability as a function of the vaccination rate, with periodic orbits presenting values of infected higher than the chaotic ones.

(ii) The second strategy is the pulsed vaccination, in which the immunization campaign operates intensively on a single day per year, more precisely and according to the simulations, just 9 h on one day in each year. The baseline vaccination rate is a small constant. Pulses are applied annually at timings given in relation to seasonality, thus modeling the campaign acting according to the transmissivity variation. The timing of the immunization pulse does not lead to a significant difference in the accumulated number of infected. Even so, acting at the inflection point of the rise in the transmissivity curve proved to be slightly more effective, reducing the percentage of susceptibles vaccinated during the pulse to result in DFE. The baseline and intense immunization rate has a linear relationship with the reduction in disease spread. Hence, the total number of cases depends on the proportion of susceptible vaccinated annually and not on independent immunization rates.

(iii) In our last strategy, we applied a pulsed width vaccination campaign. We discover that the disease spread depends on a non-linear relationship between vaccination rates and the duty cycle of the campaign. We derive the relationship between the immunization parameters that leads to the extinction of the infection within the simulated 75 years. It depends on the baseline and intensive vaccination rates, the campaign duty cycle, and the proportion of immunized newborns. We find that the reduction in the accumulated infected number depends on the annual vaccination rate of the susceptible population, this finding being valid for all three strategies, mainly in the first one. For example, regardless of the strategy, given a vaccination of $\approx 38\%$ of susceptible each year, the cumulative case of infection is reduced to only 20% of what it would be in a no-vaccination

situation. Since we study the model with normalized variables, we are always dealing with proportions of the total population. For constant population approximation, a direct transition to the number of infected people over time is valid, whereas for the more general case, where the population may vary, we must take the results into account as proportions.

We plan to study, in future works, the effects of periodic and perturbed vaccination in chaotic dynamics and bi-stable parameter ranges. In addition, we plan to fill some points opened in this work, which is exploring the effects of stochastic process in vaccination campaign.

AUTHOR DECLARATIONS

Conflict of Interest

The authors have no conflicts to disclose.

Author Contributions

Enrique C. Gabrick: Conceptualization (equal); Data curation (equal); Formal analysis (equal); Funding acquisition (equal); Investigation (equal); Methodology (equal); Project administration (equal); Resources (equal); Software (equal); Supervision (equal); Validation (equal); Visualization (equal); Writing – original draft (equal); Writing – review & editing (equal). **Eduardo L. Brugnago:** Conceptualization (equal); Data curation (equal); Formal analysis (equal); Funding acquisition (equal); Investigation (equal); Methodology (equal); Project administration (equal); Resources (equal); Software (equal); Supervision (equal); Validation (equal); Visualization (equal); Writing – original draft (equal); Writing – review & editing (equal). **Silvio L. T. de Souza:** Conceptualization (equal); Data curation (equal); Formal analysis (equal); Funding acquisition (equal); Investigation (equal); Methodology (equal); Project administration (equal); Resources (equal); Software (equal); Supervision (equal); Validation (equal); Visualization (equal); Writing – original draft (equal); Writing – review & editing (equal). **Kelly C. Iarosz:** Conceptualization (equal); Data curation (equal); Formal analysis (equal); Funding acquisition (equal); Investigation (equal); Methodology (equal); Project administration (equal); Resources (equal); Software (equal); Supervision (equal); Validation (equal); Visualization (equal); Writing – original draft (equal); Writing – review & editing (equal). **José D. Szezech, Jr.:** Conceptualization (equal); Data curation (equal); Formal analysis (equal); Funding acquisition (equal); Investigation (equal); Methodology (equal); Project administration (equal); Resources (equal); Software (equal); Supervision (equal); Validation (equal); Visualization (equal); Writing – original draft (equal); Writing – review & editing (equal). **Ricardo L. Viana:** Conceptualization (equal); Data curation (equal); Formal analysis (equal); Funding acquisition (equal); Investigation (equal); Methodology (equal); Project administration (equal); Resources (equal); Software (equal); Supervision (equal); Validation (equal); Visualization (equal); Writing – original draft (equal); Writing – review & editing (equal). **Iberê L. Caldas:** Conceptualization (equal); Data curation (equal); Formal analysis (equal); Funding acquisition (equal); Investigation (equal); Methodology (equal); Project administration (equal); Resources (equal); Software (equal); Supervision (equal); Validation (equal); Visualization (equal); Writing – original draft (equal); Writing – review & editing (equal). **Antonio M. Batista:** Conceptualization (equal); Data curation (equal); Formal analysis (equal); Funding acquisition (equal); Investigation (equal); Methodology (equal); Project administration (equal); Resources (equal); Software (equal); Supervision (equal); Validation (equal); Visualization (equal); Writing – original draft (equal); Writing – review & editing (equal). **Jürgen Kurths:** Conceptualization (equal); Data curation (equal); Formal analysis (equal); Funding acquisition (equal); Investigation (equal); Methodology (equal); Project administration (equal); Resources (equal); Software (equal); Supervision (equal); Validation (equal); Visualization (equal); Writing – original draft (equal); Writing – review & editing (equal).

DATA AVAILABILITY

Data sharing is not applicable to this article as no new data were created or analyzed in this study.

REFERENCES

[1] S. Xia, C. C. Gullickson, C. J. E. Metcalf, B. T. Grenfell, and M. J. Mina, "Assessing the effects of measles virus infections on childhood infectious disease mortality in Brazil," J. Infect. Dis. **227**, 133–140 (2023).

[2] K. A. Glatter and P. Finkelman, "History of the plague: An ancient pandemic for the age of COVID-19," Am. J. Med. **134**(2), 176–181 (2021).

[3] T. M. Tumpey, C. F. Basler, P. V. Aguilar, H. Zeng, A. Solórzano, D. E. Swayne, N. J. Cox, J. M. Katz, J. K. Taubenberger, P. Palese, and A. García-Sastre, "Spanish influenza pandemic virus," Science **310**, 77–80 (2005).

[4] C. Manchein, E. L. Brugnago, R. M. da Silva, C. F. O. Mendes, and M. W. Beims, "Strong correlations between power-law growth of COVID-19 in four continents and the inefficiency of soft quarantine strategies," Chaos **30**, 041102 (2020).

[5] M. Aguiar, S. Ballesteros, B. W. Kooi, and N. Stollenwerk, "The role of seasonality and import in a minimalistic multi-strain dengue model capturing differences between primary and secondary infections: Complex dynamics and its implications for data analysis," J. Theor. Biol. **289**, 181–196 (2011).

[6] N. Dalal, D. Greenhalgh, and X. Mao, "A stochastic model for internal HIV dynamics," J. Math. Anal. Appl. **341**, 1084–1101 (2008).

[7] L. A. Meyers, B. Pourbohloul, M. E. J. Newman, D. M. Skowronski, and R. C. Brunham, "Network theory and SARS: Predicting outbreak diversity," J. Theor. Biol. **232**(1), 71–81 (2005).

[8] L. Mao and L. Bian, "Spatial–temporal transmission of influenza and its health risks in an urbanized area," Comput. Environ. Urban Syst. **34**(3), 204–215 (2010).

[9] S. V. Scarpino and G. Petri, "On the predictability of infectious disease outbreaks," Nat. Commun. **10**, 898 (2019).

[10]S. Altizer, A. Dobson, P. Hosseini, P. Hudson, M. Pascual, and P. Rohani, "Seasonality and the dynamics of infectious diseases," Ecol. Lett. **9**, 467–484 (2006).

[11]B. Buonomo and N. Chitnis, "Seasonality in epidemic models: A literature review," Ric. di Mat. **67**, 7–25 (2018).

[12]M. B. Hoshen and A. P. Morse, "A weather-driven model of malaria transmission," Malar. J. **3**, 32 (2004).

[13]B. F. Finkenstadt and B. T. Grenfell, "Time series modelling of childhood diseases: A dynamical systems approach," J. R. Stat. Soc. Ser. C Appl. Stat. **49**(2), 187–205 (2000).

[14]N. C. Grassly and C. Fraser, "Seasonal infectious disease epidemiology," Proc. R. Soc. B: Biol. Sci. **273**(1600), 2541–2550 (2006).

[15]N. Azimaqin, Z. Pen, X. Ren, Y. Wei, and X. Liu, "Vaccine failure, seasonality and demographic changes associate with mumps outbreaks in Jiangsu Province, China: Age-structured mathematical modelling study," J. Theor. Biol. **544**, 111125 (2022).

[16]M. Aguiar, N. Stollenwerk, and B. W. Kooi, "Torus bifurcations, isolas and chaotic attractors in a simple dengue fever model with ADE and temporary cross immunity," Int. J. Comput. Math. **86**(10–11), 1867–1877 (2009).

[17]M. Mugnaine, E. C. Gabrick, P. R. Protachevicz, K. C. Iarosz, S. L. T. de Souza, A. C. L. Almeida, A. M. Batista, I. L. Caldas, J. D. Szezech Jr., and R. L. Viana, "Control attenuation and temporary immunity in a cellular automata SEIR epidemic model," Chaos, Solitons and Fractals **155**, 111784 (2022).

[18]A. M. Batista, S. L. T. de Souza, K. C. Iarosz, A. C. L. Almeida, J. D. Szezech Jr., E. C. Gabrick, M. Mugnaine, and I. L. Caldas, "Simulation of deterministic compartmental models for infectious diseases dynamics," Rev. Bras. de Ensino de Fís. **43**, e20210171 (2021).

[19]B. T. Grenfell, B. M. Bolker, and A. Kleczkowski, "Seasonality and extinction in chaotic metapopulations," Proc. R. Soc. Lond. B **259**, 97–103 (1995).

[20]M. J. Keeling and P. Rohani, *Modeling Infectious Diseases in Humans and Animals* (Princeton University Press, 2008).

[21]S. Bilal, B. K. Singh, A. Prasad, and E. Michael, "Effects of quasiperiodic forcing in epidemic models," Chaos **26**, 093115 (2016).

[22]G. Tanaka and K. Aihara, "Effects of seasonal variation patterns on recurrent outbreaks in epidemic models," J. Theor. Biol. **317**, 87–95 (2013).

[23]L. F. Olsen and W. M. Schaffer, "Chaos versus noisy periodicity: Alternative hypotheses for childhood epidemics," Science **249**, 499–504 (1990).

[24]E. C. Gabrick, E. Sayari, P. R. Protachevicz, J. D. Szezech Jr., K. C. Iarosz, S. L. T. de Souza, A. C. L. Almeida, R. L. Viana, I. L. Caldas, and A. M. Batista, "Unpredictability in seasonal infectious diseases spread," Chaos, Solitons and Fractals **166**, 113001 (2023).

[25]W. P. London and J. A. Yorke, "Recurrent outbreaks of measles, chickenpox and mumps: I. Seasonal variation in contact rates," Am. J. Epidemiol. **98**(6), 453–468 (1973).

[26]D. Greenhalgh and I. A. Moneim, "SIRS epidemic model and simulations using different types of seasonal contact rate," Syst. Anal. Model. Simul. **43**(5), 573–600 (2003).

[27]J. P. M. de Carvalho and A. A. Rodrigues, "Strange attractors in a dynamical system inspired by a seasonally forced SIR model," Physica D **434**, 133268 (2022).

[28]C. J. E. Metcalf, O. N. Bjornstad, B. T. Grenfell, and V. Andreasen, "Seasonality and comparative dynamics of six childhood infections in pre-vaccination Copenhagen," Proc. R. Soc. B **276**, 4111–4118 (2009).

[29]M. J. Keeling, P. Rohani, and B. T. Grenfell, "Seasonally forced disease dynamics explored as switching between attractors," Physica D **148**, 317–335 (2001).

[30]I. Cooper, A. Mondal, and C. G. Antonopoulos, "A SIR model assumption for the spread of COVID-19 in different communities," Chaos, Solitons and Fractals **139**, 110057 (2020).

[31]S. Ansari, M. Anvari, O. Pfeffer, N. Molkenthin, M. R. Moosavi, F. Hellmann, J. Heitzig, and J. Kurths, "Moving the epidemic tipping point through topologically targeted social distancing," Eur. Phys. J. Spec. Top. **230**, 3273–3280 (2021).

[32]B. A. Mello, "One-way pedestrian traffic is a means of reducing personal encounters in epidemics," Front. Phys. **8**, 376 (2020).

[33]E. L. Brugnago, R. M. da Silva, C. Manchein, and M. W. Beims, "How relevant is the decision of containment measures against COVID-19 applied ahead of time?," Chaos, Solitons and Fractals **140**, 110164 (2020).

[34]S. L. T. de Souza, A. M. Batista, I. L. Caldas, K. C. Iarosz, and J. D. Szezech, Jr., "Dynamics of epidemics: Impact of easing restrictions and control of infection spread," Chaos, Solitons and Fractals **142**, 110431 (2021).

[35]C. Balsa, I. Lopes, T. Guarda, and J. Rufino, "Computational simulation of the COVID-19 epidemic with the SEIR stochastic model," Comput. Math. Organ. Theory **29**, 507–525 (2023).

[36]Y. Zou, W. Yang, J. Lai, J. How, and W. Lin, "Vaccination and quarantine effect on COVID-19 transmission dynamics incorporating Chinese-Spring-Festival travel rush: Modeling and simulations," Bull. Math. Biol. **84**, 30 (2022).

[37]M. Etxeberria-Etxaniz, S. Alonso-Quesada, and M. De la Sen, "On an SEIR epidemic model with vaccination of newborns and periodic impulsive vaccination with eventual on-line adapted vaccination strategies to the varying levels of the susceptible subpopulation," Appl. Sci. **10**(22), 8296 (2020).

[38]M. De la Sen, S. Alonso-Quesada, A. Ibeas, and R. Nistal, "On a discrete SEIR epidemic model with two-doses delayed feedback vaccination control on the susceptible," Vaccines **9**(4), 398 (2021).

[39]M. Voyseym, S. A. Clemens, S. Madhi, L. Weckx, P. Folegatti, P. Aley, B. Angus, V. Baillie, S. Barnabas, Q. Bhorat, S. Bibi, C. Briner, P. Cicconi, E. Clutterbuck, A. Collins, C. Cutland, T. Darton, K. Dheda, and C. Chritina, "Single-dose administration and the influence of the timing of the booster dose on immunogenicity and efficacy of ChAdOx1 nCoV-19 (AZD1222) vaccine: A pooled analysis of four randomised trials," The Lancet **397**, 881–891 (2021).

[40]H. A. Thompson, A. B. Hogan, P. G. T. Walker, P. Winskill, I. Zongo, I. Sagara, H. Tinto, J. B. Ouedraogo, A. Dicko, D. Chandramohan, B. Greenwood, M. Cairns, and A. C. Ghani, "Seasonal use case for the RTS,S/AS01 malaria vaccine: A mathematical modelling study," Lancet Glob. Health **10**, e1782–e1792 (2022).

[41]N. A. M. Molinari, I. R. Ortega-Sanchez, M. L. Messonnier, W. W. Thompson, P. M. Wortley, E. Weintraub, and C. B. Bridges, "The annual impact of seasonal influenza in the US: Measuring disease burden and costs," Vaccine **25**(27), 5086–5096 (2007).

[42]M. J. Keeling and B. T. Grenfell, "Understanding the persistence of measles: Reconciling theory, simulation and observation," Proc. R. Soc. Lond. Ser. B: Biol. Sci. **269**(1489), 335–343 (2002).

[43]S. Gao, Y. Liu, J. J. Nieto, and H. Andrade, "Seasonality and mixed vaccination strategy in an epidemic model with vertical transmission," Math. Comput. Simul. **81**, 1855–1868 (2011).

[44]C. Atchison, B. Lopman, and W. J. Edmunds, "Modelling the seasonality of rotavirus disease and the impact of vaccination in England and Wales," Vaccine **28**, 3118–3126 (2010).

[45]B. Shulgin, L. Stone, and Z. Agur, "Pulse vaccination strategy in the SIR epidemic model," Bull. Math. Biol. **60**, 1123–1148 (1998).

[46]E. C. Gabrick, P. R. Protachevicz, A. M. Batista, K. C. Iarosz, S. L. T. de Souza, A. C. L. Almeida, J. D. Szezech, Jr., M. Mugnaine, and I. L. Caldas, "Effect of two vaccine doses in the SEIR epidemic model using a stochastic cellular automaton," Physica A **597**, 127258 (2022).

[47]J. Duarte, C. Januário, N. Martins, J. M. Seoane, and M. A. F. Sanjuán, "Controlling infectious diseases: The decisive phase effect on a seasonal vaccination strategy," Int. J. Bifurcat. Chaos **31**(15), 2130044 (2021).

[48]X. Wang, H. Pen, B. Shi, D. Jiang, S. Zhang, and B. Chen, "Optimal vaccination strategy of a constrained time-varying SEIR epidemic model," Commun. Nonlinear Sci. Numer. Simul. **67**, 37–48 (2019).

[49]Z. Bai and Y. Zhou, "Global dynamics of an SEIRS epidemic model with periodic vaccination and seasonal contact rate," Nonlinear Anal. Real World Appl. **13**, 1060–1068 (2012).

[50]I. A. Moneim and D. Greenhalgh, "Use of a periodic vaccination strategy to control the spread of epidemics with seasonally varying contact rate," Math. Biosci. Eng. **2**(3), 591–611 (2005).

[51]S. H. Ho, D. He, and R. Eftimie, "Mathematical models of transmission dynamics and vaccine strategies in Hong Kong during the 2017–2018 winter influenza season," J. Theor. Biol. **476**, 74–94 (2019).

[52]C. J. E. Metcalf, J. Lessler, P. Klepac, F. Cutts, and B. T. Grenfell, "Impact of birth rate, seasonality and transmission rate on minimum levels of coverage needed for rubella vaccination," Epidemiol. Infect. **140**(12), 2290–2301 (2012).

[53]D. J. Nokes and J. Swinton, "The control of childhood viral infections by pulse vaccination," J. Math. Appl. Med. Biol. **12**, 29–53 (1995).

26 January 2024 00:00:50

[54] Z. Agur, L. Cojocaru, G. Mazor, R. M. Anderson, and Y. L. Danon, "Pulse mass measles vaccination across age cohorts," Proc. Natl. Acad. Sci. U.S.A. **90**, 11698–11702 (1993).

[55] J. D. Grabenstein and R. L. Nevin, "Mass immunization programs: Principles and standards," in *Mass Vaccination: Global Aspects—Progress and Obstacles. Current Topics in Microbiology and Immunology* (Springer, Berlin, Heidelberg, 2006), Vol 304.

[56] A. K. Alkhamis and M. Hosny, "A synthesis of pulse influenza vaccination policies using an efficient controlled elitism non-dominated sorting genetic algorithm (CENSGA)," Electronics **11**(22), 3711 (2022).

[57] P. Song, Y. Lou, and Y. Xiao, "A spatial SEIRS reaction–diffusion model in heterogeneous environment," J. Differ. Equ. **267**, 5084–5114 (2019).

[58] K. L. Cooke, "Analysis of an SEIRS epidemic model with two delays," J. Math. Biol. **35**, 240–260 (1996).

[59] O. N. Bjørnstad, *Epidemics: Models and Data Using R* (Springer, 2018).

[60] J. D. Hernández Guillén, A. Martín del Rey, and L. Hernández Encinas, "Study of the stability of a SEIRS model for computer worm propagation," Physica A **479**, 411–421 (2017).

[61] T. Tél and M. Gruiz, *Chaotic Dynamics: An Introduction Based on Classical Mechanics* (Cambridge University Press, 2006).

[62] R. M. Anderson and R. M. May, *Infectious Diseases of Humans: Dynamics and Control* (Oxford University Press, 1992).

[63] C. L. Wesley and L. J. S. Allen, "The basic reproduction number in epidemic models with periodic demographics," J. Biol. Dyn. **3**(2–3), 116–129 (2009).

[64] G. Meinsma, "Elementary proof of the Routh-Hurwitz test," Syst. Control Lett. **25**(4), 237–242 (1995).

[65] A. Mclean and R. Anderson, "Measles in developing countries. Part II. The predicted impact of mass vaccination," Epidemiol. Infect. **100**(3), 419–442 (1988).

[66] F. Henderson Fenner, Z. Jezek, and I. D. Ladnyi, and World Health Organization, "Smallpox and its eradication," History Int. Public Health **6**, 1371–1409 (1988), available at https://www.aphl.org/programs/preparedness/Smallpox/pdf/9241561106.pdf.

[67] S. Bagcchi, "The World's largest COVID-19 vaccination campaign," Lancet Infect. Dis. **21**(3), 323 (2021).

[68] J. C. Butcher, *The Numerical Analysis of Ordinary Differential Equations: Runge-Kutta and General Linear Methods* (Wiley, Wiley-Interscience, 1987).

[69] E. S. Medeiros, I. L. Caldas, M. S. Baptista, and U. Feudel, "Trapping phenomenon attenuates the consequences of tipping points for limit cycles," Sci. Rep. **7**, 42351 (2017).

[70] K. T. Alligood, T. D. Sauer, and J. A. Yorke, *Chaos: An Introduction to Dynamical Systems* (Springer, 1996).

26 January 2024 00:00:50